Ezequiel J. López[1]
Professor
Departamento de Mecánica Aplicada,
Facultad de Ingeniería,
U. N. del Comahue, CONICET,
Buenos Aires 1400,
Neuquén Q8300IBX, Argentina
e-mail: ezequiel.lopez@fain.uncoma.edu.ar

Carlos A. Wild Cañón
Departamento de Mecánica Aplicada,
Facultad de Ingeniería,
U. N. del Comahue,
Buenos Aires 1400,
Neuquén Q8300IBX, Argentina
e-mail: chiquito_wc@hotmail.com

Sofía S. Sarraf
Professor
Departamento de Mecánica Aplicada,
Facultad de Ingeniería,
U. N. del Comahue, CONICET,
Buenos Aires 1400,
Neuquén Q8300IBX, Argentina
e-mail: sofia.sarraf@fain.uncoma.edu.ar

A Constant-Pressure Model for the Overlap of Chambers in Rotary Internal Combustion Engines

In this work, a constant-pressure model capable to simulate the overlap of chambers in rotary internal combustion engines is proposed. It refers as a chamber overlap when two adjacent chambers are in communication through the same port, which could occur in some rotary internal combustion engines. The proposed model is thermodynamic (or zero-dimensional (0D)) in nature and is designed for application in engine simulators that combine one-dimensional (1D) gasdynamic models with thermodynamic ones. Since the equations of the proposed model depend on the flow direction and on the flow regime, a robust and reliable solution strategy is developed. The model is assessed using a two-dimensional (2D) problem and is applied in the simulation of a rotary internal combustion engine. Results for this last problem are compared with other common approaches used in the simulation of rotary engines, showing the importance of effects such as the interaction between overlapping chambers and the dynamics of the flow.
[DOI: 10.1115/1.4033744]

1 Introduction

For decades, the use of software dealing with the simulation of internal combustion engines has been useful to its design and optimization. Engine simulators, which apply thermodynamic (or 0D) models in conjunction with 1D gasdynamic models for the simulation of pipes, are specially useful due to the possibility of simulating the whole machine at a low computational cost. As a mirror of the industry for internal combustion engines, the development of models and software was mainly focused on reciprocating engines. At present, there are many commercial software designed for performance simulation of these engines. However, there is not available specific software developed for rotary engines aside from the attempts made in the decades of 1970s, 1980s, and 1990s for the Wankel engine [1–6]. This lack of codes for the simulation of rotary engines led researchers to propose strategies for the prediction of the performance of rotary engines applying software designed for the simulation of reciprocating engines [7,8].

However, there are special features of many rotary engines which could be very difficult, if not impossible, to simulate by using models developed for alternative engines. One of such features is the gas exchange process. Most rotary internal combustion engines use ports for the gas exchange processes. Generally, these ports are located in the housing and are shared by the operative chambers, which would lead to the "overlap" of the adjacent chambers. It is referred as "chamber overlap" to the situation when two adjacent chambers are intercommunicated through the same port and, hence, also with the pipe end connected to the port. For instance, Fig. 1 shows a sketch of the Wankel rotary engine where the overlap of two chambers during the exhaust process can be observed. Depending on the port geometry, this overlap could occur also during the intake. The overlap of chambers is never found in piston engines, since each individual cylinder has its own valves and ports.

The overlap of adjacent chambers could be an important aspect in order to design optimal intake and exhaust systems. For example, when a given chamber is beginning the exhaust process, it overlaps with its adjacent (leading) chamber, which is ending the exhaust phase. The first chamber will enter to the blowdown phase and part of the exhausted gas could enter to the other chamber, thereby producing an increment in the chamber pressure and in the mass of burnt gases. Due to the interaction with the states at the chambers, the overlap could modify the pressure at the end of

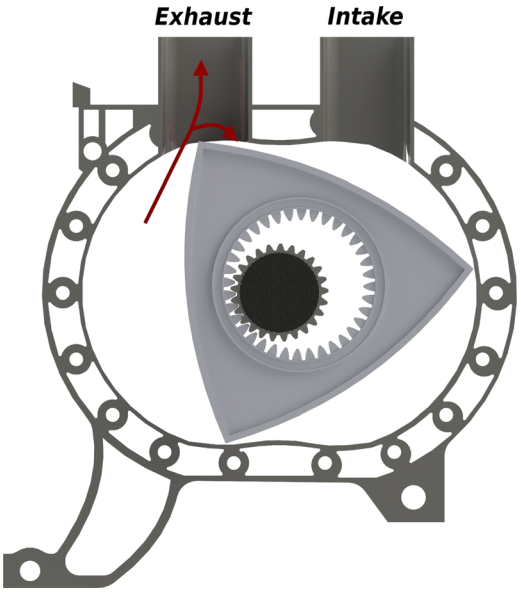

Fig. 1 Outline of a Wankel engine during the chamber overlap in the exhaust port

[1]Corresponding author.

Contributed by the IC Engine Division of ASME for publication in the JOURNAL OF ENGINEERING FOR GAS TURBINES AND POWER. Manuscript received December 9, 2013; final manuscript received May 27, 2016; published online June 28, 2016. Editor: David Wisler.

the pipes in connection with the ports and also alter the propagation of pressure waves along the manifolds.

Another characteristic of many rotary engines is that all chambers share the same intake pipe and the same exhaust pipe. In contrast, reciprocating engines use manifolds with branches which lead to each cylinder. In some multicylinder-reciprocating engines, these branches could be shared by two adjacent cylinders, but in these cases, the dephasing in the cycle of these nearby cylinders assures that its intake or exhaust processes will not overlap.

Whereas that take into account the fact that all chambers employ the same intake pipe and the same exhaust pipe could be easily solved at the code implementation level, the overlap of chambers needs to be modeled. Chamber overlap was not yet addressed in the literature and, therefore, the consequent interaction of the chambers state with the pressure waves in the intake and exhaust pipes were not considered in the simulations of rotary engines. Yamamoto [9] notices the issue of chamber overlap in the Wankel engine, but does not discuss the impact over the engine performance. The first works dealing with the simulation of Wankel engines did not simulate the flow along the pipes assuming the intake and exhaust pipes as plenums [1–3]. Certainly, this hypothesis prevents the simulation of dynamic effects in the intake and exhaust systems. Another common approach is to consider individual chambers, each one isolated from the remaining ones and having its own intake and exhaust pipes [7,8]. In this proposal, it is possible to simulate dynamic pressure waves in the intake and exhaust systems, but the chamber overlap is not considered.

The overlap of chambers also could take place in the constant-volume combustion rotary engine (MRCVC, by Motor Rotativo de Combustiòn a Volumen Constante) engine [10] as illustrated in Fig. 2. This engine is composed by a rotor and n vanes inside a cylindrical housing ($n \geq 2$). For instance, Fig. 2 shows the geometry of an MRCVC with three vanes. The central region of the housing and the vanes has oval shape, with apex seals to avoid gas leakage. The rotor is a ring with cylindrical hollows allowing the relative rotation of the vanes. Each vane must keep parallel its centerline with respect to the other vanes while their centers revolve around the output shaft. This kinematic constraint is accomplished by means of a rim, which also links the engine shaft with the rotor and the vanes. Breathing is performed through ports in the side housings and/or through lateral ports in the center housing. The main feature of the MRCVC engine is that the minimum volume of the chamber extends by an angular interval greater than zero. This geometric feature enables to perform the combustion process partially or totally at constant volume. Therefore, since the combustion chamber has a surface area/volume ratio similar to those found in reciprocating engines [11], a net increment on the engine thermodynamic efficiency is expected. Moreover, the MRCVC has a perfect static and dynamic balance of its moving components, allowing to achieve high smoothness and low engine vibration. Also, the contact between apex seals and walls is harmonic, which would permit to reduce wear and noise. The duration of one operating cycle is [12]

$$\Delta\varphi = (1 + 2/n)360\,\text{deg} \tag{1}$$

in terms of the rotating angle of the output shaft and, since there are $n+2$ operating chambers, n power pulses occur for each output shaft revolution. Currently, this rotary engine is in the design stage, which was the motivation for the present study.

In the present work, a constant-pressure 0D model for the simulation of the overlap of chambers is proposed. The formulation of the model is presented for the general case with $M \geq 1$ chambers in communication with a pipe end, where each chamber connects to the pipe end through a restriction that represents a port or a valve. For the particular case with two chambers, which is applicable to the modeling of chamber overlap in rotary internal combustion engines, a strategy for the resolution of the nonlinear equation system is proposed.

The article is organized as follows. First, the equations of the model are stated. Second, the solution strategy developed for the case of two chambers is described. In Sec. 4, the numerical results are showed, including the assessment of the 0D model using a multidimensional model. In addition, the application of the proposed strategy to the 0D/1D simulation of an MRCVC engine and the comparison with other common strategies are presented. In Sec. 5, conclusions are drawn.

2 Constant-Pressure Model for Chamber Overlap

The proposed model is a generalization of the constant-pressure valve model developed by Benson [13]. A complete description of this valve model can be found in Refs. [14] and [15]. In this model, the restriction imposed to the flow by the port-valve system is modeled as a convergent nozzle, where the nozzle throat represents the minimum cross-sectional area. The flow through this nozzle is assumed isentropic and stationary (instantaneous), while the gas is modeled as ideal. Since the state at the pipe end connected to the chamber (or cylinder) through the valve is part of the unknowns, the outgoing characteristic lines are included in the set of equations.

In the general case, M chambers in connection with a unique pipe are considered. Each chamber has its own port or valve and

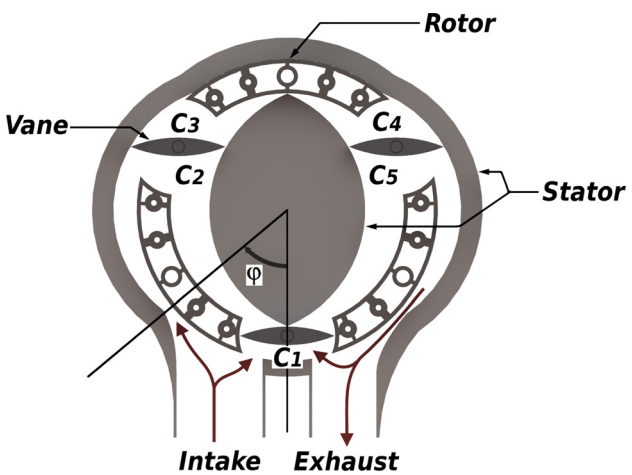

Fig. 2 Outline of an MRCVC engine during the chamber overlap in the intake and exhaust ports

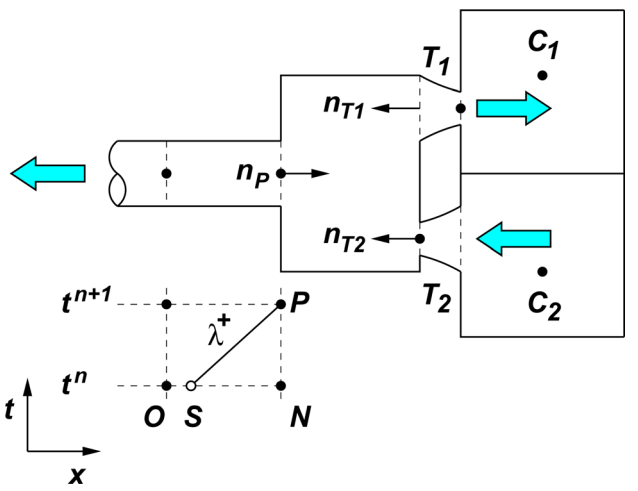

Fig. 3 Sketch of two chambers in connection with a pipe. Definitions of the points considered in the proposed model and orientation of normals.

its own state. For instance, Fig. 3 shows a sketch for the case of two chambers connected to a pipe. This case represents the model which is applied to simulate the chamber overlap that occurs during the breathing processes in rotary engines. Chambers C_1 and C_2 in Fig. 3 are connected to the right pipe end through two convergent nozzles with throats T_1 and T_2, respectively, representing the restriction to the flow imposed by the port. A possible flow direction is indicated in this figure with thick arrows. The pipe is modeled as 1D and the remaining components are represented with 0D models.

Figure 3 includes a portion of the mesh in the space-time plane x–t at the right pipe end. It is assumed that the solution is known at all mesh nodes at time t^n and it is solved for time $t^{n+1} = t^n + \Delta t$, where Δt is the time-step that satisfies the Courant–Friedrichs–Levy (CFL) condition [16]. In Fig. 3, the point N corresponds to the pipe end at time t^n, while point P is in the same spatial position at time t^{n+1}. The point O represents the first interior point at left of the pipe end at time t^n. In what follows, subscripts indicate the evaluation point. Figure 3 also shows a scheme of the Mach line λ^+, which propagates with speed $u + a$, where u is the flow velocity and a is the sound speed. This characteristic line is approximated by a straight line from point S to point P, where the spatial position of S is such that $x_N - x_S = (u_S + a_S)\Delta t$ and the state at this point is linearly interpolated between the states at points O and N. The CFL condition assures that point S always lays between O and N. Note that in the case depicted in Fig. 3, the exterior unit normal to the pipe end is $n_P = +1$. For the opposite pipe end, the exterior unit normal is $n_P = -1$ and the characteristic line to be considered is λ^-, which propagates with speed $u - a$. Therefore, the first equation proposed for the model is the compatibility equation along the Mach line $\lambda^{\text{sign}(n_P)}$. This equation is integrated to first-order of accuracy, giving [14]

$$u_P^* = -\frac{p_P - p_S}{\rho_S a_S} + u_S \cdot n_P - \text{RHS}_2^{\text{sign}(n_P)} \tag{2}$$

where $u_P^* = u_P \cdot n_P$, p is the pressure, ρ is the density, and

$$\text{RHS}_2^{\pm} = \left[-(k-1)\left(\frac{\dot{q}_S}{\rho_S a_S} \pi \frac{D_S}{F_S} + \frac{u_S}{a_S} G_S \right) \pm G_S + \frac{u_S a_S}{F_S} \frac{dF}{dx}\bigg|_S \right] \Delta t$$

In the last expression, k is the gas-specific heat ratio, F is the cross-sectional area of the pipe, D is the equivalent diameter of the pipe, $\dot{q}$ is the heat flux through the pipe wall, and

$$G = f \frac{u|u|}{2} \pi \frac{D}{F}$$

is the specific friction force, with the friction coefficient given by $f = 2\tau_w/\rho u$, τ_w being the viscous shear stress at the pipe wall.

The second equation is the mass conservation between flows at the nozzles and the pipe end

$$\rho_P u_P^* + \sum_{j=1}^{M} \rho_{T_j} \psi_{T_j} u_{T_j}^* = 0 \tag{3}$$

where $\psi_{T_j} = F_{T_j}/F_P$, F_{T_j} being the cross-sectional area of the nozzle throat corresponding to the jth port, and $u_{T_j}^* = u_{T_j} \cdot n_{T_j}$. n_{T_j} is the exterior unit normal to the cross-sectional surface at the throat of the jth nozzle (see Fig. 3). Note that $n_{T_j} = -n_P$, $j = 1, \ldots, M$.

When the flow is entering to the pipe, i.e., $u_P^* < 0$, it is proposed to use the energy conservation between flows at the nozzles and the pipe end. For the opposite flow direction ($u_P^* > 0$), the compatibility equation along the pathline λ^0 must be considered. This characteristic curve propagates with speed u [16]. Hence, the third equation is written as follows:

$$\begin{cases} \rho_P u_P^* \left[a_P^2 + \delta (u_P^*)^2 \right] \\ \quad + \sum_{j=1}^{M} \rho_{T_j} \psi_{T_j} u_{T_j}^* \left[a_{T_j}^2 + \delta \left(u_{T_j}^* \right)^2 \right] = 0 & \text{if } u_P^* < 0 \\ \left(\dfrac{p_P}{p_R} \right)^{1/k} = \dfrac{\rho_P}{\rho_R} \exp(\text{RHS}_1) & \text{if } u_P^* \geq 0 \end{cases} \tag{4}$$

where $\delta = (k-1)/2$ and

$$\text{RHS}_1 = \left[\frac{k-1}{a_R^2} \left(\frac{\dot{q}_R}{\rho_R} \pi \frac{D_R}{F_R} + u_R G_R \right) \right] \Delta t$$

Point R is defined for λ^0 in an analogous way as point S was defined for $\lambda^{\pm}$.

For each nozzle, it is assumed that the flow expands isentropically from the stagnation state while it flows through the nozzle until the throat is reached. Hence, for $j = 1, \ldots, M$

$$\begin{cases} \dfrac{p_P}{p_{T_j}} = \left(\dfrac{\rho_P}{\rho_{T_j}} \right)^k & \text{if } u_{T_j}^* < 0 \\ \dfrac{p_{C_j}}{p_{T_j}} = \left(\dfrac{\rho_{C_j}}{\rho_{T_j}} \right)^k & \text{if } u_{T_j}^* \geq 0 \end{cases} \tag{5}$$

Here, the subscript C_j refers to the chamber in communication with the jth port.

For all nozzles, the energy conservation between the corresponding stagnation state and the nozzle throat is written as follows:

$$\begin{cases} a_P^2 + \delta (u_P^*)^2 = a_{T_j}^2 + \delta (u_{T_j}^*)^2 & \text{if } u_{T_j}^* < 0 \\ a_{C_j}^2 = a_{T_j}^2 + \delta (u_{T_j}^*)^2 & \text{if } u_{T_j}^* \geq 0 \end{cases} \tag{6}$$

Finally, the conditions at the nozzle throats close the set of equations for the proposed model. For $j = 1, \ldots, M$, these conditions are posed as follows

If the flow is subsonic at T_j

$$\begin{cases} p_{T_j} = p_{C_j} & \text{if } u_{T_j}^* < 0 \\ p_{T_j} = p_P \left[1 + \delta \left(\dfrac{u_P^*}{a_P} \right)^2 \right]^{k/(k-1)} & \text{if } u_{T_j}^* \geq 0 \end{cases} \tag{7}$$

If the flow at T_j is choked

$$|u_{T_j}^*| = a_{T_j} \tag{8}$$

Then, if the state in each chamber is known, it is straightforward to see that Eqs. (5)–(7) [or Eq. (8)] form a set of $3M$ equations which, in conjunction with Eqs. (2)–(4), form a nonlinear system for the $3(M+1)$ unknowns ρ_P, u_P, p_P, ρ_{T_j}, u_{T_j}, p_{T_j}, $j = 1, \ldots, M$.

3 Solution Methodology for the Case of Two Chambers

The main difficulty for the resolution of the equation system arising from the proposed model is that the equations to be solved depend on the direction of the flow at the pipe end and on the flow regime and direction at the nozzle throats. One possibility is to solve the system of $3(M+1)$ equations simultaneously. This strategy was applied in another work for the case $M = 1$, i.e., the original valve model, using a convex combination in order to take into account the transition between subsonic and sonic regimes at the nozzle throat [15]. Even though this strategy works well in some

Table 1 Possible flow directions and flow regimes at the throat of the nozzles in the case $M = 2$

Case	u_P^*	$u_{T_1}^*$	$u_{T_2}^*$	$\lvert u_{T_1}^* \rvert / a_{T_1}$	$\lvert u_{T_2}^* \rvert / a_{T_2}$
1	<0	<0	>0	<1	<1
2 (1)	<0	>0	<0	<1	<1
3	<0	>0	>0	<1	<1
4	>0	<0	>0	<1	<1
5 (4)	>0	>0	<0	<1	<1
6	>0	<0	<0	<1	<1
7	<0	<0	>0	=1	<1
8	<0	>0	<0	=1	<1
9	<0	>0	>0	=1	<1
10	>0	<0	>0	=1	<1
11	>0	>0	<0	=1	<1
12	>0	<0	<0	=1	<1
13 (8)	<0	<0	>0	<1	=1
14 (7)	<0	>0	<0	<1	=1
15 (9)	<0	>0	>0	<1	=1
16 (11)	>0	<0	>0	<1	=1
17 (10)	>0	>0	<0	<1	=1
18 (12)	>0	<0	<0	<1	=1
19	<0	<0	>0	=1	=1
20 (19)	<0	>0	<0	=1	=1
21	<0	>0	>0	=1	=1
22	>0	<0	>0	=1	=1
23 (22)	>0	>0	<0	=1	=1
24	>0	<0	<0	=1	=1

cases, it was found that its robustness is weak and highly dependent on the initialization procedure.

Hence, a solution method for the system (2)–(7) [or (8)] for the case of two chambers ($M = 2$) is presented. The method is also applicable to the case of a unique chamber, i.e., $M = 1$. A special strategy for the resolution of the case $M = 2$ was developed because it corresponds to the problem of chamber overlap in some rotary engines, such as the Wankel and the MRCVC engines. The strategy was inspired in the approach followed by Benson in the application of boundary conditions for the flow through a valve or a port [13]. The idea is to split the problem in different cases. For each case, an allowed direction for the involved flow velocities is assumed as well as a flow regime at the nozzle throats. Table 1 lists the possible cases for $M = 2$. Although there are 24 possible cases, due to symmetry considerations, only 14 different cases must be solved. These 14 cases are indicated in bold in Table 1, while for the remaining ten cases, the corresponding symmetric case is indicated between brackets. In addition, it is assumed that the states into the chambers are known, generally from the previous time-step.

For each case, the system of nine equations is algebraically handled in order to get a unique nonlinear equation with only one unknown. This unknown was selected as the nondimensional flow velocity at the pipe end. Each nonlinear equation is solved applying the Newton–Raphson method with an Armijo line-search strategy in order to get global convergence [17]. Of course, this strategy is impractical for $M > 2$, but has proven to be robust and reliable for $M = 1$ and $M = 2$.

The separation in cases as proposed in Table 1 translates partially the problem to the choice of the corresponding case. For each time-step in the simulation, it is started with a list whose elements are the possible cases of solution. These cases are a subset of the cases listed in Table 1. Some cases are discarded by the pressure ratio between the chambers, since its value is known a priori. Other cases may be ruled out imposing the condition of no flow reversal during the time-step, for instance, when any of the throats are choked. The first case in the list is the case solved in the previous time-step. Then, the algorithm tries to solve the cases contained in the resulting list, starting from the first element of the list. The case which is trying to be solved is temporarily labeled as potential case of solution (PCS). If the convergence of the nonlinear equation for the PCS is not achieved, the PCS is removed from the list and the following element in the list, which represents another possible case, is adopted as a new PCS. When the nonlinear equation for a given PCS is successfully solved, the solution is checked to fulfill the assumptions made for the case in regard to the flow direction and the regime at throats. If these assumptions are satisfied, the PCS is adopted as the solution case for the current time-step; if not, another case from the list is tested.

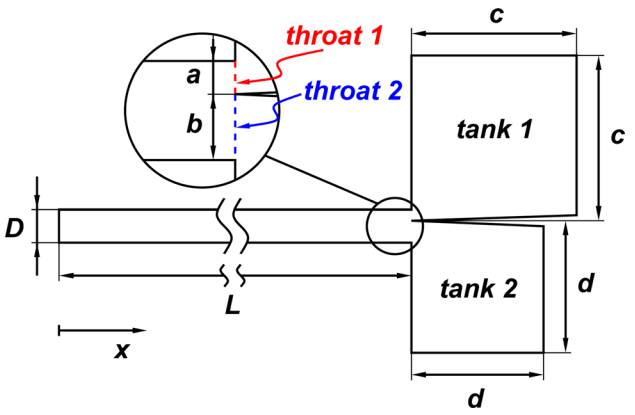

Fig. 4 Scheme of the geometry of the 2D problem. $L = 500$ mm, $D = 30$ mm, $a = 10$ mm, $b = 20$ mm, $c = 150$ mm, $d = 120$ mm.

4 Results

The proposed model was implemented in the internal combustion engine simulator ICESym [18], using the solution methodology presented in Sec. 3 for both, $M = 1$, 2. Since the goal is to compare the proposed model with other approaches used in the literature, first the new model is tested in a 2D case.

4.1 Discharge of Two Tanks to the Atmosphere. Even though the aim of this article is to apply the proposed model in the simulation of rotary internal combustion engines, this test presents a situation with similar characteristics to the exhaust processes in those engines. The problem consists in two tanks connected with the atmosphere through a straight pipe, as shown in Fig. 4. The geometry of the problem is assumed 2D. From the point of view of the model, the unique difference with respect to an internal combustion engine is that the discharge port areas of the tanks are constant.

The dimensions of the pipe and tanks are indicated in the caption of Fig. 4. The ports of tanks 1 and 2 are identified as throats 1 and 2, respectively, because these flow sections represent the throats of the convergent nozzles in the 0D model. Atmospheric conditions are $p_a = 100$ kPa and $T_a = 300$ K. The gas is modeled as ideal, with specific gas constant $R = 276$ J/kg K and specific heat ratio $k = 1.28$. Initially, the gas is at rest in the whole domain. Inside the pipe, the gas pressure is 130 kPa and the temperature is 1000 K. The gas state inside tank 1 is $p_1 = 340$ kPa and $T_1 = 1500$ K, while inside tank 2, the state is $p_2 = 160$ kPa and $T_2 = 1200$ K. Both the gas properties and the initial states were set to values that can be found in an exhaust process in an internal combustion engine. At $t = 0$, the left pipe end is suddenly open to the atmosphere, as well as the ports of the tanks. Pressure at the left pipe end is kept equal to p_a during the simulation, and the walls of the pipe and tanks are isolated. The flow is assumed inviscid, and the simulation lasts for $t = 7.18$ ms.

First, the problem is solved with a 2D model using the computational fluid dynamics (CFDs) module of the code PETSc-FEM [19]. The domain is discretized with a mesh of 62,273 triangular elements and 31,944 nodes. The time-step used in the simulation is $\Delta t = 2.5 \times 10^{-6}$ s.

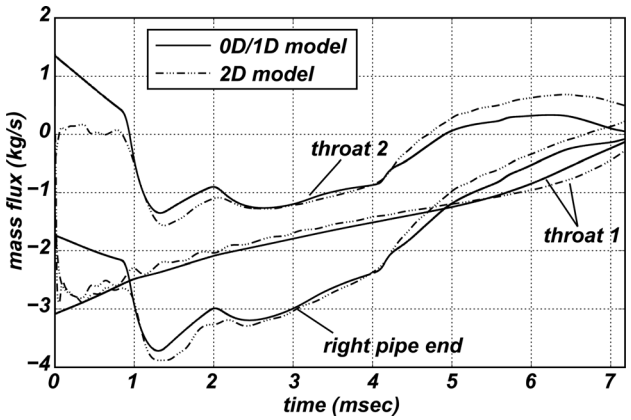

Fig. 5 Comparison of the mass flux per unit length through throats 1 and 2, and the right pipe end computed with the 0D/1D model and the 2D model for the problem of the discharge of two tanks to the atmosphere

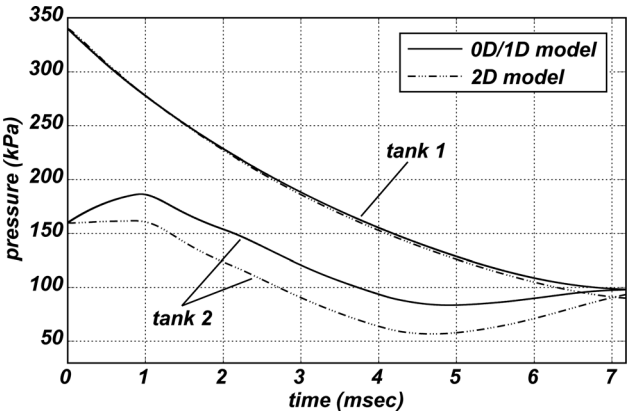

Fig. 7 Comparison of the pressure into the tanks computed with the 0D/1D model and the 2D model for the problem of the discharge of two tanks to the atmosphere

In the second place, the problem is solved using 0D/1D models. The pipe is modeled as a 1D domain, where the governing equations are the Euler equations of gasdynamics with the addition of source terms in order to account for viscous friction with the pipe wall, the heat transfer through the pipe wall, and variations of the cross-sectional area of the pipe along its axis [15]. Euler equations are discretized in space with the finite volume method (FVM) using a total variation diminishing (TVD) scheme. In particular, the method by Harten [20] is applied (see Ref. [21] for details). Time derivatives are discretized applying the forward Euler difference scheme. Tanks are simulated with a 0D model, and the coupling between tanks and the right pipe end is solved applying the model proposed in this work. The pipe is discretized using equal length elements of 3 mm, while the time-step is computed according the CFL condition with a CFL number of 0.5. The discharge coefficients of the throats were computed using the results obtained with the 2D model. Since they vary along the simulation, time average values of these discharge coefficients are used. Also, it is distinguished between discharge coefficients for inflow (C_d^{in}) and outflow (C_d^{out}). For throat 1, $C_{d,1}^{\text{in}} = C_{d,1}^{\text{out}} = 0.88$, while for throat 2, $C_{d,2}^{\text{in}} = 0.58$ and $C_{d,2}^{\text{out}} = 0.86$. It must be pointed out that a single value for the discharge coefficient is very restrictive for use in this transient problem and it could directly affect the performance of the proposed model.

Now, the results from the 0D/1D model are compared with the corresponding ones to the 2D model. The comparison is made at throats, at tanks, and at the right pipe end. For the 2D model, the state for the right pipe end is computed at a distance $D/3 = 10\,\text{mm}$ from the plane of the throats. Figure 5 shows the mass flux per unit length computed at the throats and at the right pipe end. The proposed model captures the reversal of the flow through the throat 2 and the trends in the three analyzed sections. The implications of the use of a constant discharge coefficient can be observed in the figure, in particular for the throat 2, where the value of $C_{d,2}^{\text{in}}$ is too high in the first part of the simulation ($t < 1\,\text{ms}$), but somewhat low when the flow reverses again after $t = 4.6\,\text{ms}$ approximately.

Figures 6 and 7 exhibit the density and pressure into the tanks, respectively. A good agreement is observed for tank 1, where the maximum error is at the end of the simulation with values of 2.98% in the density and 9.07% in the pressure. Before $t = 5.5\,\text{ms}$, approximately, the error in these variables is below 1%. The state of the gas into the tank 2 computed with the 0D/1D model separates from the value determined with the 2D model due to the overestimated mass flux at the beginning of the simulation. This higher mass flux increments the mass and pressure into the tank 2, setting a difference with the values corresponding to the 2D model, which is held for $t > 1\,\text{ms}$.

It is concluded that the proposed model works relatively fine and is able to capture the main features of the problem. However, in order to obtain a better approximation to the state of gas inside the tank 2, it should be considered a variable discharge coefficient with, for instance, the pressure ratio.

4.2 Simulation of the Gas Exchange Processes in an MRCVC Engine. In this subsection, some numerical results of the application of the proposed model to the simulation of the

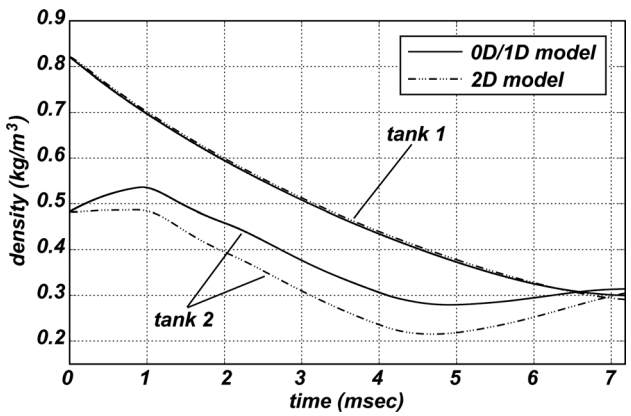

Fig. 6 Comparison of the density into the tanks computed with the 0D/1D model and the 2D model for the problem of the discharge of two tanks to the atmosphere

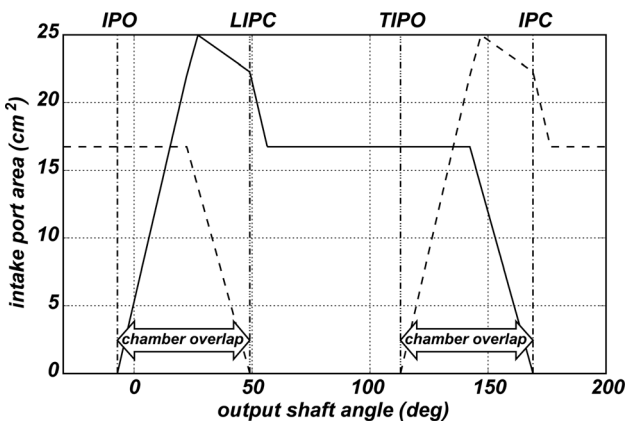

Fig. 8 Area of the intake port as a function of the output shaft angle φ. The periods of chamber overlap are indicated. Leading chamber IPC (LIPC), trailing chamber IPO (TIPO).

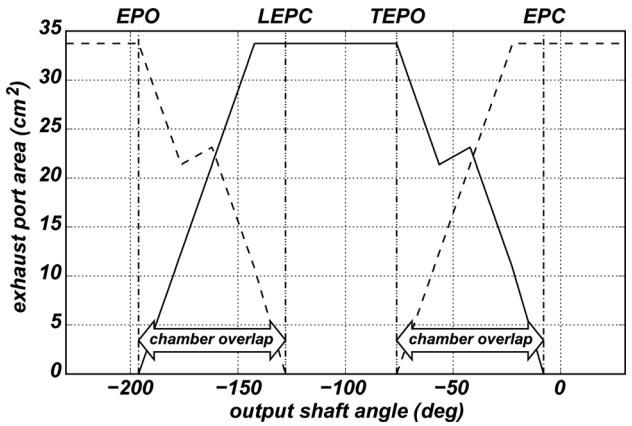

Fig. 9 Area of the exhaust port as a function of the output shaft angle φ. The periods of chamber overlap are indicated. Leading chamber EPC (LEPC), trailing chamber EPO (TEPO).

breathing processes in the MRCVC engine are presented. The operating principles of the MRCVC engine and a description of its theoretical advantages can be found in Refs. [11] and [12]. The present study is focused on the intake and exhaust processes; therefore, other important models for the simulation of the MRCVC engine, such as the geometric model, the heat transfer model, the heat release model, etc., are not discussed.

The engine simulated is naturally aspirated, spark-ignited, and, for each speed, it works at full load. The engine has $n = 3$ vanes (see Fig. 2), a maximum volume of the chamber of 500 cm^3, and compression ratio $r_c = 9$. For this case, the cycle extends for 600 deg of the engine shaft rotation φ (see Eq. (1)) and there are five operative chambers [12]. Angles are taken relative to the chamber at the "TC" (top center) position. Figure 2 shows the chamber 1 (C1) at this position, i.e., when $\varphi = 0$ deg. In the simulated case, ports are located in the center housing, as outlined in Fig. 2. The opening and closing events of the ports relative to the reference angle are the following: intake port opening (IPO): −7.068 deg, intake port closing (IPC): 169.05 deg, exhaust port opening (EPO): −196.22 deg, exhaust port closing (EPC): −7.9286 deg. Figures 8 and 9 show, respectively, the areas of the intake and exhaust ports as a function of φ. In these figures, the port areas for the "leading" and "trailing" chambers are also shown, and the periods of chamber overlap are indicated. The length of the intake runner is 1.2 m and its diameter is 70 mm. The exhaust pipe has 0.8 m in length and 50 mm in diameter. The flow in these pipes is modeled with the 1D Euler equations for gasdynamics, which are solved with a TVD–FVM scheme, as explained in Sec. 4.1. Discharge coefficients for intake and exhaust ports are assumed constant, with values of 0.75 for the intake port and 0.7 for the exhaust port. These values for the discharge coefficients were taken from the literature about the Wankel engine simulation (see, e.g., Ref. [1]), due to the lack of data for the MRCVC engine. Although those values may not closely correspond to the port geometry of an MRCVC, they are useful to the purpose of this work, consisting in comparing the proposed model with some conventional strategies applied in the literature for the gas exchange process simulation in rotary engines.

The operating gas has specific gas constant $R = 287$ J/kg K and specific heat ratio $k = 1.3$. The fuel is iso-octane and the fuel/air mixture is stoichiometric. Chambers are modeled with a thermodynamic single-zone model, where the combustion is modeled using the Wiebe function [22], assuming that it starts at $\varphi = 267$ deg and lasts for 60 deg. Heat transfer is modeled using the correlation proposed by Annand, which was applied for the simulation of the Wankel engine [23]. The temperature of the chamber wall is assumed constant at 450 K. Crevice flow and leakages are not considered. At the pipe ends communicated with the atmosphere, the atmospheric density and the total pressure are imposed when the flow is entering the pipe. In the case of outgoing flow from the pipe, only the atmospheric pressure is imposed at the pipe end.

The following results correspond to a constant engine speed of 6000 rev/min. Figure 10 shows the pressure inside one of the chambers during its intake phase (from the IPC angle to the IPO angle) and the pressure in the corresponding overlapping chambers. The figure also includes the static pressure at the pipe end in communication with the chambers. The followed chamber is identified as chamber 1, while the overlapping chambers are denoted with the number 2. At IPO, the residual gas inside chamber 1 has a pressure greater than the pressure at the intake port, which produces the expansion of this residual mass toward the intake pipe. Toward the IPC angle of the leading chamber, a compression wave that arrives at the intake port produces the increment of the pressure inside chamber 1. This wave reflects as an expansion wave that travels to the opposite pipe end. The pressure inside the chamber 1 falls below the intake port pressure due to the chamber volume is increasing. The maximum chamber volume is reached at $\varphi = 150$ deg, where starts the compression "stroke" producing the increment of pressure inside chamber 1 at the final of the intake process.

For the exhaust phase in one of the chambers, Fig. 11 shows the pressure inside the chambers and the pressure at the corresponding pipe end. When the exhaust port opens, the blowdown produces an increment of the pressure at the exhaust port. This process continues until $\varphi = -150$ deg, approximately, when the chamber

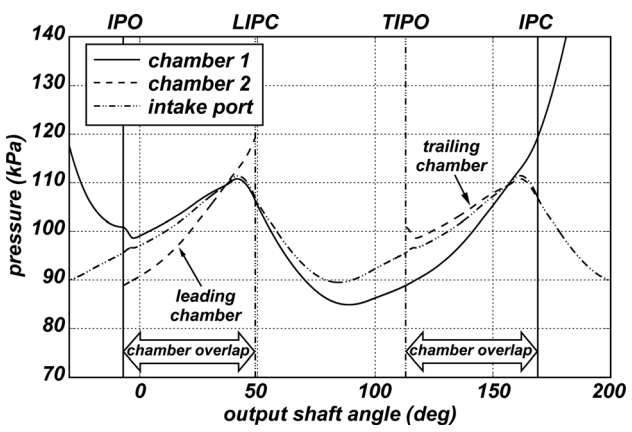

Fig. 10 Pressure along the intake phase of a chamber. Speed: 6000 rev/min. The followed chamber is labeled with the number 1 and the overlapping chambers with the number 2.

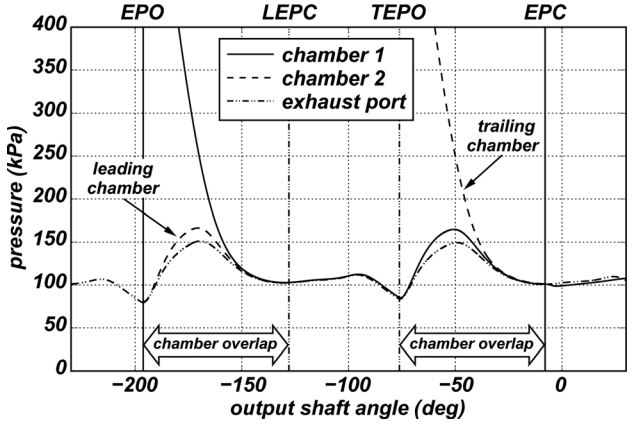

Fig. 11 Pressure along the exhaust phase of a chamber. Speed: 6000 rev/min. The followed chamber is labeled with the number 1 and the overlapping chambers with the number 2.

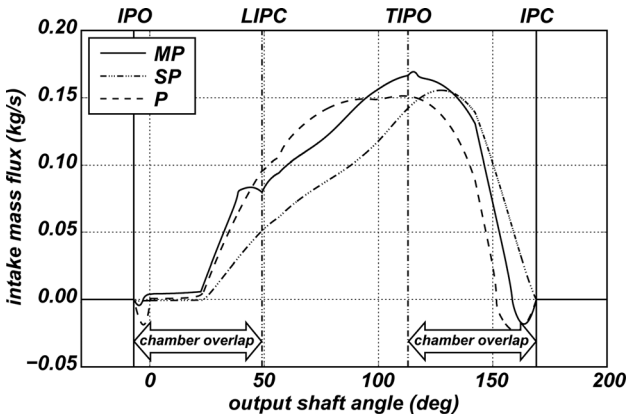

Fig. 12 Mass flux through the intake port computed with different approaches. Speed: 6000 rev/min.

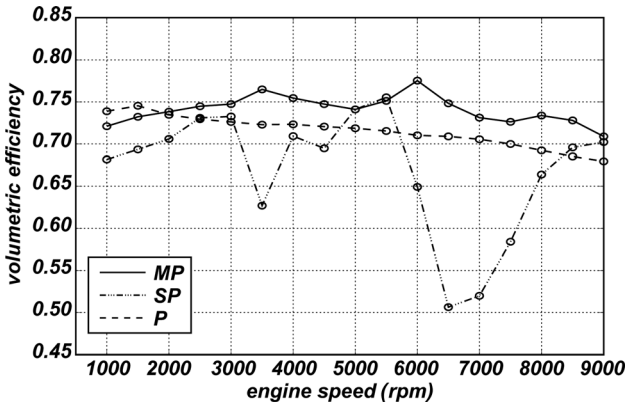

Fig. 14 Volumetric efficiency as a function of the engine speed

reaches the maximum volume. After this angle, the displacement phase proceeds at almost constant pressure until an expansion wave arrives to the exhaust port. This scavenge wave cannot be fully exploited because the opening of the exhaust port of the trailing chamber, which begins its blowdown phase, promotes the rise of the pressure at the exhaust port and inside the chamber 1. Gas pressure inside chamber 1 peaks close to $\varphi = -50$ deg and then decreases until the EPC angle.

The results obtained with the proposed model are compared with the common approaches used in the Wankel literature for the simulation of the flow through ports. In one of such approaches, the manifolds are considered to be infinite plenums, and a quasi-steady compressible flow model is used to evaluate the mass exchange between the chambers and manifolds [2]. The intake and exhaust pressures for this last strategy are generally averages of measured values in running engines. Since experimental data for the MRCVC engine are not available, the mean pressures at the intake and exhaust ports were computed from the results obtained with the model presented in this work. Then, a variable state with the engine speed is computed at the exhaust port, where the corresponding values are the result of the average of the total pressure and the density at the port along the cycle for each engine speed. This strategy is named P (Plenum). In the second common approach, individual chambers with their own ports and intake and exhaust pipes are considered [7,8]. This last strategy can account for dynamic effects in the intake and exhaust ducts, but neglects the interaction between contiguous chambers. The strategy is named isolated chamber model, and it is referred as single port (SP).

In Fig. 12, the mass flux through the intake port computed with the present model (identified as MP, multiport) is showed, where

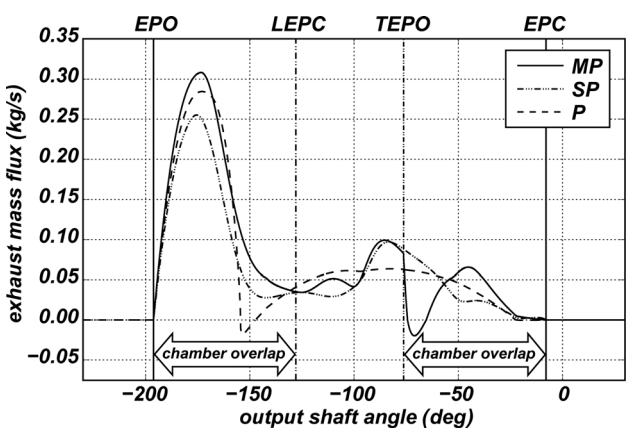

Fig. 13 Mass flux through the exhaust port computed with different approaches. Speed: 6000 rev/min.

a positive value indicates that the mass is entering to the chamber. When the intake port opens, a backflow of residual mass is produced due to the fact that the pressure inside the chamber is higher than the pressure at port (see Fig. 10). During the constant-volume period of the chamber ($|\varphi| \leq 22.32$ deg), the mass flux is low and then increases due to the rise of the intake port pressure and the growth of the chamber volume. The maximum intake mass flux is reached, approximately, when the trailing chamber opens its intake port. At the end of the intake phase, a reverse flow of fresh charge from the chamber to the intake pipe occurs due to the compression of the gas inside the chamber. Figure 12 also includes the intake mass flux obtained with the other two approaches. The lack of dynamic effects in the strategy P is evident. The isolated chamber model presents the lowest values of mass flux in the first part of the intake process due to dephasing of the waves that come to the port. In this case, it is predicted that no backflow at the end of the intake process because of the delayed compression wave that arrives to the port.

Figure 13 shows the mass flux through the exhaust port for the present model and the other two alternatives. In this figure, a positive mass flux means gas flowing from the chamber to the exhaust port. The three models predict a different peak mass flow rate during the blowdown, although the extension of this phase is similar for all models. Along the displacement process, the models MP and SP show oscillations in the exhaust mass flux curve due to dynamic effects. In the case of the MP model, notice the re-entry of burnt gas to the chamber due to the EPO of the trailing chamber.

From the results previously presented, it is evident that the performance of the gas exchange systems predicted by the considered models will vary significantly. For instance, Fig. 14 shows the volumetric efficiency as a function of the engine speed, where the reference density is the atmospheric one. In general, the present model predicts the highest values for the volumetric efficiency with two peaks at 3500 and 6000 rev/min, which are result of dynamic effects. The volumetric efficiency computed with the SP model presents large fluctuations due to the dephasing of the pressure waves in the intake system for some engine speeds.

5 Conclusion

A constant-pressure 0D model capable to simulate the overlap of chambers in rotary internal combustion engines was proposed. The model is a generalization of a constant-pressure valve model proposed in the literature. These kind of models lead to systems of nonlinear equations that could change equations depending on the direction and regime of the flow, which represents a drawback for the solution strategies. A robust and reliable solution methodology was developed, which is useful for the case of one or two chambers in communication with a pipe. The proposed model was assessed in a 2D problem consisting in two tanks discharging to

the atmosphere through a straight pipe. The results were compared with the ones computed with a 2D model, where a good agreement was found, particularly for the state at one of the tanks and for the mass flux. In addition, the proposed model was used to compute the gas exchange processes in a rotary engine and it was compared with other common approaches applied in the literature. Quite different results were obtained with the models, which is attributed to the no consideration of the chamber overlap and the unsuitable representation of the dynamic effects. A more comprehensive evaluation of the model is needed, using multidimensional CFD results and experimental measurements.

Acknowledgment

This work has received financial support from Consejo Nacional de Investigaciones Científicas y Técnicas (CONICET, Argentina), Universidad Nacional del Comahue (UNCo, Argentina, Grant No. 04/I215), Agencia Nacional de Promoción Científica y Tecnológica (ANPCyT, Argentina, Grant No. PICT–2014–2460) and was performed with the *Free Software Foundation/GNU-Project* resources such as GNU–Linux-OS, GNU–GFortran, GNU–Octave, and GNU–Git, as well as other Open Source resources as Python, Cython, NETGEN, Xfig, and LATEX.

References

[1] Danieli, G., 1976, "A Performance Model of a Wankel Engine, Including the Effects of Burning Rates, Heat Transfer, Leakage and Quenching Compared With Measured Pressure Time Histories," Ph.D. thesis, Massachusetts Institute of Technology, Cambridge, MA.
[2] Norman, T., 1983, "A Performance Model of a Spark Ignition Wankel Engine: Including the Effects of Crevice Volumes, Gas Leakage, and Heat Transfer," Master's thesis, Massachusetts Institute of Technology, Cambridge, MA.
[3] Roberts, J., 1985, "Heat Release Estimation and Prediction of Wankel Stratified-Charge Combustion Engine," Master's thesis, Massachusetts Institute of Technology, Cambridge, MA.
[4] Bartrand, T., and Willis, E., 1990, "Performance of a Supercharged Direct-Injection Stratified-Charge Rotary Combustion Engine," Technical Report No. NASA TM–1990-103105.
[5] Kim, K., Chae, J., and Chung, T., 1991, "A Performance Simulation for Spark Ignition Wankel Rotary Engine," SAE Technical Paper No. 912479.
[6] Bartrand, T., and Willis, E., 1993, "Rotary Engine Performance Computer Program User's Guide," Technical Report No. NASA CR–1993-191192.
[7] Handschuh, R., and Owen, A., 2010, "Analysis of Apex Seal Friction Power Loss in Rotary Engines," NASA Glenn Research Center, Cleveland, OH, Technical Report No. TM–2010-216353.
[8] Tartakovsky, L., Baibikov, V., Gutman, M., and Veinblat, M., 2012, "Simulation of Wankel Engine Performance Using Commercial Software for Piston Engines," SAE Technical Paper No. 2012-32-0098.
[9] Yamamoto, K., 1981, *Rotary Engine*, Sankaido, Tokyo, Japan.
[10] Toth, J., 2004, "Motor Rotativo de Combustión a Volumen Constante (MRCVC)," Patent Res. No. AR004806B1, Rec. No. P 19960105411.
[11] Toth, J., Di Nezio, J., Staniscia, C., and López, E., 2000, "Ventajas mecánicas y termodinámicas de un nuevo motor rotativo," 9 Congreso Chileno de Ingeniería Mecánica, pp. 1–6.
[12] López, E., 2009, "Methodologies for the Numerical Simulation of Fluid Flow in Internal Combustion Engines," Ph.D. thesis, Facultad de Ingeniería y Ciencias Hídricas, Universidad Nacional del Litoral, Santa Fe, Argentina.
[13] Benson, R., 1982, *The Thermodynamics and Gas Dynamics of Internal-Combustion Engines*, Vol. 1, Clarendon Press, Oxford, UK.
[14] Alessandri, M., 2000, "Simulazione della fase di ricambio della carica in un motore benzina ad iniezione diretta," Master's thesis, Dipartamento di Ingegneria Meccanica, Facolta' di Ingegneria, Universita' degli Studi di Roma Tor Vergata, Rome, Italy.
[15] López, E., and Nigro, N., 2010, "Validation of a 0D/1D Computational Code for the Design of Several Kind of Internal Combustion Engines," Lat.-Am. Appl. Res., **40**(2), pp. 175–184.
[16] Hirsch, C., 1990, *Numerical Computation of Internal and External Flows, Volume 2: Computational Methods for Inviscid and Viscous Flows*, Wiley, Chichester, UK.
[17] Papalambros, P., and Wilde, D., 2000, *Principles of Optimal Design: Modeling and Computation*, 2nd ed. , Cambridge University Press, Cambridge, UK.
[18] Nigro, N., López, E., and Gimenez, J., 2010–2016, "ICESym. An Internal Combustion Engine Simulator."
[19] Storti, M., Nigro, N., Paz, R., Dalcín, L., López, E., Battaglia, L., and Ríos Rodríguez, G., 1999–2016, "PETSc-FEM. A General Purpose, Parallel, Multi-Physics FEM Program."
[20] Harten, A., 1983, "A High Resolution Scheme for the Computation of Weak Solutions of Hyperbolic Conservation Laws," J. Comput. Phys., **49**(3), pp. 357–393.
[21] López, E., and Nigro, N., 2011, "Computational Simulation of In-Cylinder Flows in Internal Combustion Engines by Means of the Coupling of Zero-/One-Dimensional and Multidimensional Codes," Mecánica Computacional, Vol. 30, pp. 403–423.
[22] Heywood, J., 1988, *Internal Combustion Engine Fundamentals*, McGraw-Hill, New York.
[23] Ramos, J., 1989, *Internal Combustion Engine Modeling*, Hemisphere, New York.